RSC Advances

ROYAL SOCIETY OF CHEMISTRY

www.rsc.org/advances

Journal Name

RSCPublishing

ARTICLE

The Effect of Carbon Black in Carbon Counter Electrode for $CH_3NH_3PbI_3/TiO_2$ heterojunction solar cells

Cite this: DOI: 10.1039/x0xx00000x

Received 00th January 2015,
Accepted 00th January 2015

DOI: 10.1039/x0xx00000x

www.rsc.org/

Heng Wang*, Xiaoyan Hu, Hongxia Chen

Carbon counter electrodes (CCEs) based on pure flacky graphite, pure carbon black and graphite/carbon black composites were respectively applied in mesoscopic $CH_3NH_3PbI_3/TiO_2$ heterojunction solar cells. Crystallinity, conductivity and current-voltage characterisitcs were measured to study the influence of carbon black in the graphite/carbon black CEs on the perovskite crystal and the photovolatic performance of devices. Results showed that the content of carbon black in CCEs could significantly affect the crystallinity and uniformity of the perovskite crystal, leading to different photovolatic performance of the devices. The device with the optimized content of carbon black showed an efficiency of 7.08%, which was much higher than the efficiency of 2.75% obtained by the device based on graphite CE without carbon black.

Introduction

In the past few years, lead halide perovskite solar cells have experienced the fastest increase in reported efficiencies ever achieved for any photovoltaic technology. In the early development, lead halide perovskite solar cells were fabricated with liquid electrolyte and showed low efficiencies[1,2]. In 2012, the first solid-state perovskite solar cell with an impressive efficiency of 9.7% was reported[3]. Soon after, lots of efforts were devoted to solid-state perovskite solar cell[4-7]. Up to now, efficiencies over 15% have been obtained by many groups[8-12], which makes it a promising candidate of the next generation photovoltaic technology. However, the conventional counter electrodes (CEs) of perovskite solar cells are fabricated with noble metals under high vaccum conditions, which significantly increase the overall cost of the devices. Therefore, it is worth developing cost-effective CE for perovskite solar cells. In 2013, Han's group reported the using carbon counter electrode (CCE) to fabricate a $CH_3NH_3PbI_3/TiO_2$ heterojunction solar cell, which showed a PCE of 6.64%[13]. In that work, $CH_3NH_3PbI_3$ was directly deposited in a $TiO_2/ZrO_2/C$ triple layer scaffold from CH_3NH_3I and PbI_2 presusor solution. In 2014, a novel mixed-cation perovskite $(5\text{-}AVA)_x(MA)_{1-x}PbI_3$ was filled into $TiO_2/ZrO_2/C$ scaffold and an impressive PCE of 12.84% was achieved for perovskite solar cells based on CCE[14]. Also perovskite solar cells based on CCE using flaky graphite with different sized were reported[15]. Usually, the CCEs are made by screen-printing or doctror-blading technic with graphite and carbon black as main components[16,17]. Compared with conventional noble metal CEs, CCEs are more cost-effective due to their cheaper materails and easier processing methods. Moreover, because perovskite crystals form directly in a mesocopic $TiO_2/ZrO_2/C$ scaffold for perovskite solar cells based on CCEs, the structure of the CCE films directly affect the particle size and uniformity of perovskite crystal[13,15], which have great influence on the photovoltaic performance of perovskite solar cells[18]. Although CCE is a promising candidate for perovskite solar cells, few relevant studies on CCE for perovskite solar cells were reported. In this work, we studied the effect of carbon black in graphite/carbon black composite CEs on the photovolatic performance for mesoscopic $CH_3NH_3PbI_3/TiO_2$ heterojunction solar cells. The crystallinity and uniformity of perovskite crystals deposited on different CCEs based on flacky graphite, amorphous carbon black and graphite/carbon black composite were investigated respectively. For devices, current-voltage characteristics measurements were carried out to study the influence of the carbon black on the device performance. Results showed that carbon black in CCEs could weaken the crystallinity of $CH_3NH_3PbI_3$ crystal and improve the uniformity of the perovskite film, leading to increased photovolatic performance.

Experimental

Fabrication of carbon pastes. Graphite paste: 2 g flaky graphite powder (8000 mesh) and 0.2 g ethyl cellulose were added into 10 g terpineol. Carbon black paste: 2 g carbon black powder (30 nm) and

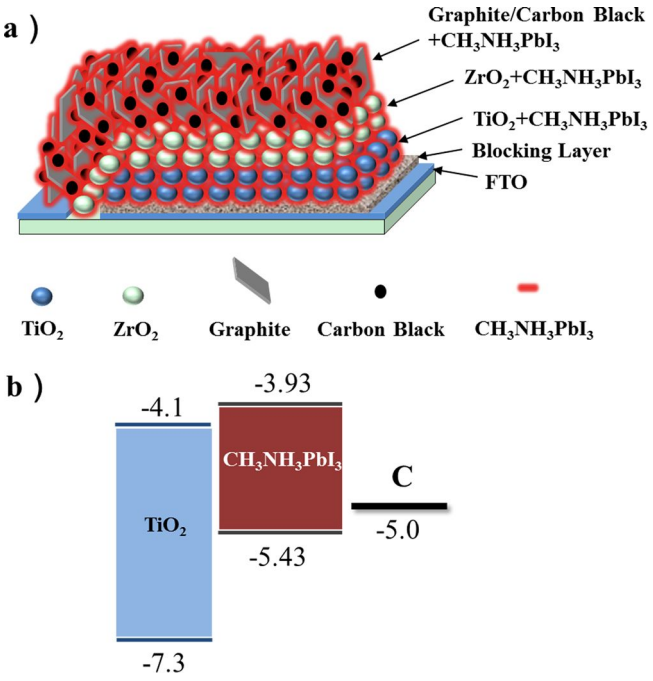

Fig. 1 a) A schemed structure of $CH_3NH_3PbI_3/TiO_2$ heterojunction solar cells based on CCE. b) The corresponding energy levels of TiO_2, $CH_3NH_3PbI_3$ and Carbon.

0.2 g ethyl cellulose were added into 10 g terpineol. Graphite/carbon black paste (20% content of carbon black): 1.6 g graphite powder, 0.4 g carbon black powder and 0.2 g ethyl cellulose were added into 10 g terpineol. All the three mixture were followed by ball milling for 2 h.

Fabrication of mesoscopic perovskite solar cells. The fluorine-The fluorine-doped SnO_2 substrates were etched with laser to form two detached electrode pattern before being cleaned ultrasonically cleaned with detergent, deionized water and ethanol respectively. After that the patterned substrates were coated with a 100 nm compact TiO_2 layer by aerosol spray pyrolysis at 450 °C. Then a 1 μm nanoporous TiO_2 layer was deposited on the compact TiO_2 layer by screen printing with a TiO_2 slurry and sintered at 500 °C for 30 min. And then, a ZrO_2 layer and a carbon film were printed on the top of the nanoporous TiO_2 layer successively, and sintered at 400 °C for 30 min, forming a porous $TiO_2/ZrO_2/C$ scaffold. The thicknesses of ZrO_2 layer and carbon layer were around 1 μm and 5 μm respectively. Finally, a 20 μl $CH_3NH_3PbI_3$ precursor (0.1 g CH_3NH_3I and 0.29 g PbI_2 were mixed in 1 mL γ-butyrolactone) was dipped on the top of each $TiO_2/ZrO_2/C$ scaffold. Finally, the substrates were dried at 60 °C for 20 min in air under dark, resulting in the completion of devices.

Characterization. The cross section of the devices and the top views of different CCEs were imaged by a field-emission scanning electron microscope (FE-SEM). The XRD spectra of the prepared films were tested by a x-ray diffraction system (85 PANalytical Empyrean, Cu Kα radiation; λ=1.5418 Å). The square resistances of CCEs with different contents of carbon black were tested by four-probe measurement. Current–voltage characterization was performed using a Keithley 2400 source meter under simulated AM 1.5 sunlight illumination (100 mW cm^{-2}) provided by an Oriel solar simulator (Model 9119X, Newport Co.). The illuminated active

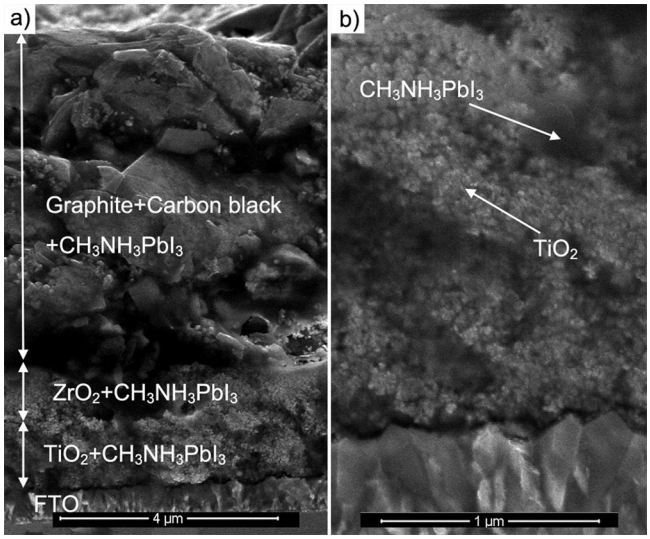

Fig. 2 a) The SEM cross section of a $TiO_2/CH_3NH_3PbI_3$ heterojunction perovskite solar cell based on CCE. b) The high magnification $TiO_2/CH_3NH_3PbI_3$ layer.

area of photovoltaic measurements was 0.13 cm^{-2}. Incident photon-currentconversion efficiency (IPCE) was recorded on a DC Power Meter (Model 2931-C, Newport Co.) under irradiation of a 300W xenon lamp light source with a motorized monochromator (Oriel). The xenon lamp was powered by an Arc Lamp Power Supply (Model69920, Newport Co.).

Results and Discussion

Structure of $TiO_2/CH_3NH_3PbI_3$ heterojunction perovskite solar cells based on CCEs. Fig 1a shows a schemed structure of a $TiO_2/CH_3NH_3PbI_3$ heterojunction perovskite solar cell based on CCE where nanoporous TiO_2 layer, ZrO_2 insulating layer and carbon layer were screen-printed on FTO/compact TiO_2 substrate layer by layer. $CH_3NH_3PbI_3$ was filled in the pores of $TiO_2/ZrO_2/C$ triple layer films by one-step solution method from PbI_2 and CH_3NH_3I precursor. **Fig 1b** shows the energy levels of TiO_2, $CH_3NH_3PbI_3$ and C respectively. **Figs 2a** and **b** show the SEM cross section of a $TiO_2/CH_3NH_3PbI_3$ heterojunction perovskite solar cell and its high magnification $TiO_2/CH_3NH_3PbI_3$ layer, respectively. In **Fig 2a**, it is clear that 1 μm TiO_2 layer, 1 μm ZrO_2 layer and 5 μm carbon layer are ordinarily deposited on the surface of FTO glass. From **Fig 2b**, we could see that $CH_3NH_3PbI_3$ is filled in the pores of nanoporous TiO_2, and the bright region and dark region represent TiO_2 and $CH_3NH_3PbI_3$ respectively.

Characterization of $CH_3NH_3PbI_3$ crystal deposited on different carbon films. We deposited three different carbon films on glasses by screen-printing with graphite paste, carbon black paste, and graphite/carbon black paste respectively. After sintering at 400 °C for 30 min, the thicknesses of the films were around 5 μm. Then a precursor solution of PbI_2 and CH_3NH_3I was dropped on each of the three different carbon films and dried at 60 °C to forming $CH_3NH_3PbI_3$ perovskite crystal. **Figure 3a**, **b** and **c** show the SEM sections of the three carbon films respectively. The particle sizes of flaky graphite distribute from hundreds of nanometres to several microns (**Fig 3a**) and the particle size of carbon black is tens of nanometres (**Fig 3c**). **Figure 3d**, **e** and **f** show the SEM section of

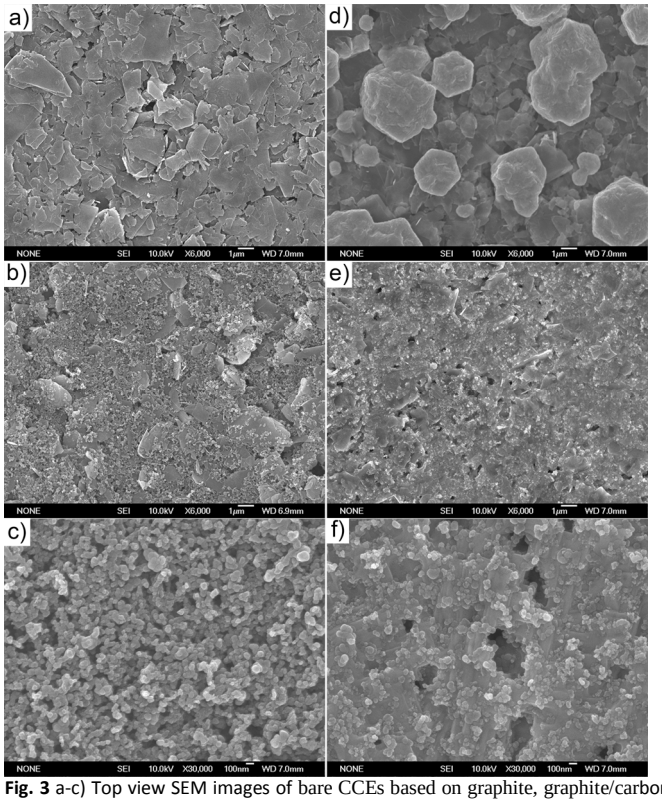

Fig. 3 a-c) Top view SEM images of bare CCEs based on graphite, graphite/carbon black and carbon black, respectively. d-f) Top view SEM images of the three corresponding CCEs infilrated with $CH_3NH_3PbI_3$ from precursor solution of PbI_2 and CH_3NH_3I.

$CH_3NH_3PbI_3$ perovskite crystals deposited on the three different carbon films respectively. From **Fig 3d** we could see that $CH_3NH_3PbI_3$ deposited on graphite film show inhomogeneous morphology and show wide crystallite sizes distribution from hundreds of nanometres to several mirons. From **Fig 3e** and **f** we could see that $CH_3NH_3PbI_3$ deposited on carbon films containing carbon black show uniform and compact crystalline film, and no large crystallite was observed. This could be attributed that the nanoporous structure of carbon black limited the growth of $CH_3NH_3PbI_3$ crystal.

In order to understand the effect of carbon black in CCEs on the crystallinity of $CH_3NH_3PbI_3$ perovskite crystal, we carried out x-ray diffraction (XRD) patterns of $CH_3NH_3PbI_3$ deposited on the three carbon films and on bare glass, which were compared in **Fig 4**. The diffraction peaks near 27° and 55° are the main characteristic peaks of flaky graphite. The diffraction peaks at the lattice planes of (110), (220), (310), (224) and (314) are the main characteristic peaks of $CH_3NH_3PbI_3$ deposited on bare glass. Among the three carbon films, $CH_3NH_3PbI_3$ deposited on carbon black film show the weakest diffraction intensities at most of the main characteristic peaks. And the diffraction intensities of $CH_3NH_3PbI_3$ on carbon black film are even weaker than that on bare glass. This could be attributed that the nanoporous structure of carbon black could limit the growth of PbI_2 and $CH_3NH_3PbI_3$ successively, resulting in decreased crystallinity. And among the three carbon films, $CH_3NH_3PbI_3$ deposited on graphite film show the strongest diffraction intensity at most of the main characteristic peaks. This is consistent with the large particle

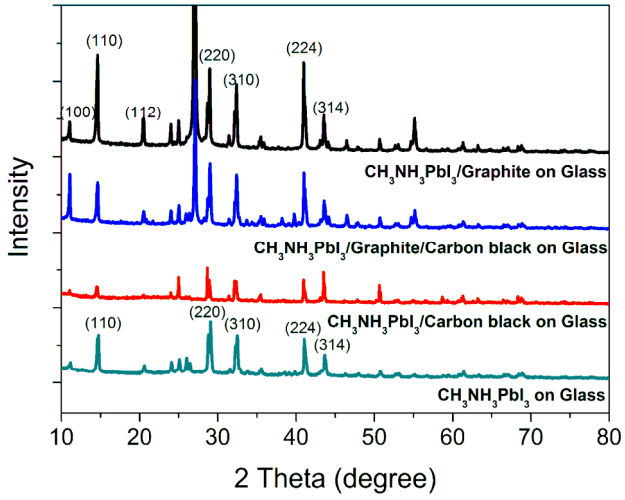

Fig. 4 XRD patterns of $CH_3NH_3PbI_3$ deposited on three carbon CCEs based on graphite, graphite/carbon black and carbon black and $CH_3NH_3PbI_3$ deposited on bare glass is also displayed.

size of $CH_3NH_3PbI_3$ on graphite film which could be seen from **Fig 3d**. Compared with $CH_3NH_3PbI_3$ on graphite film, $CH_3NH_3PbI_3$ on graphite/carbon black film exhibit decreased diffraction intensity at most of the characteristic peaks except the peak of (100). The decreased diffraction intensity of $CH_3NH_3PbI_3$ for graphite/carbon black film could be due to the limitation effect of the nanoporous structure of carbon black.

Characterization of devices with different contents of carbon black in CCEs. The photocurrent density-voltage curves of $TiO_2/CH_3NH_3PbI_3/C$ devices with different contents of carbon black in CCEs are displayed in **Fig. 5.** The photovoltaic performance of devices with different contents of carbon black in CCEs are displayed in **Table 1.** The device based on pure graphite CE showed poor photovoltaic characteristics with open-circuit voltage (V_{oc}), short-circuit current density (J_{sc}), fill factor(*FF*) and power conversion efficiency (*PCE*) of 753 mV, 6.96 mA cm^{-2}, 0.53 and 2.75% respectively. The photovoltaic performances of devices were improved with the increase of carbon black contents in CCEs. When 10% content of carbon black was induced into CCEs, V_{oc}, J_{sc} and *PCE* of the device were increased to 844 mV, 12.45 mA cm^{-2} and 5.54% respectively. The best performance of the devices was obtained when the contents of carbon black was 20% in CCEs, which exhibited a V_{oc} of 867 mV, a J_{sc} of 15.24 mA cm^{-2} and an efficiency of 7.08%. However, when the contents of carbon black were further increased, the efficiencies of devices were decreased. The device with 30% content of carbon black showed a V_{oc} of 871 mV, a J_{sc} of 14.34 mA cm^{-2}, a *FF* of 0.52 and a *PCE* of 6.44%. And the device based on pure carbon black CE obtained a V_{oc} of 839 mV, a J_{sc} of 9.85 mA cm^{-2} and a FF of 0.30, resulting in a poor efficiency of 2.46%. The improved performances for devices with low contents of carbon black in CCEs could be attributed to the improved uniformity of perovskite film, which was subsequently critical to efficient perovskite solar cells[11]. The poor performance for device with 100% content of carbon black in CCEs could be due to the poor conductivity of pure carbon black CEs since poor conductivity of CEs could directly lead to low *FF* value for the device[19].

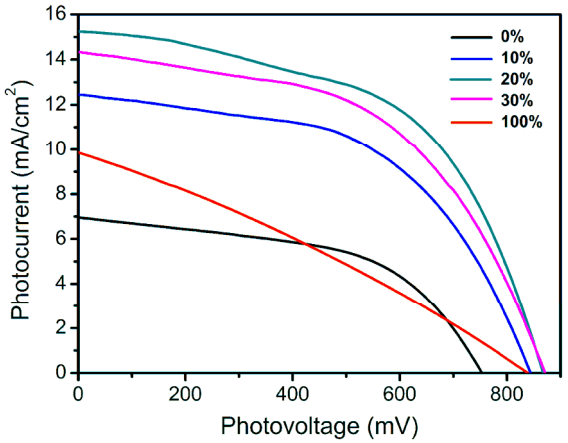

Fig. 5 Photocurrent density-voltage curves of devices based on CCEs with different contents of carbon black under standard simulated AM 1.5 illumination of 1000 W m^{-2}.

Table 1 Photovoltaic performance of TiO_2/$CH_3NH_3PbI_3$/C devices with different contents of carbon black in CCEs under AM1.5 conditions 100mW·cm^{-2}. The thickness of TiO_2, ZrO_2 and C films are ~1 μm, ~1 μm and ~5 μm respectively.

contents (wt%)	J_{sc} /mA·cm^{-2}	V_{oc}/mV	*FF*	*PCE*(%)
0%	6.96	753	0.53	2.75
10%	12.45	844	0.53	5.54
20%	15.24	867	0.54	7.08
30%	14.34	871	0.52	6.44
100%	9.85	839	0.30	2.46

In order to investigate the effect of carbon black on J_{sc} of the devices, we measured the IPCE curves of the devices. **Fig. 6** shows IPCE curves for devices based on CEs with 0%, 30% and 100% contents of carbon black respectively. The integrated photocurrents calculated from the overlap integral of the IPCE spectra with the AM 1.5 solar emission are also shown in **Fig. 6**. The integrated photocurrents for devices based on CEs with 0%, 30% and 100% contents of carbon black are 6.48 mA cm^{-2}, 13.45 mA cm^{-2} and 9.26 mA cm^{-2} respectively. These results are close to the Jsc of 6.96 mA cm^{-2}, 14.34 mA cm^{-2} and 9.85 mA cm^{-2} obtained by the initial I-V testing respectively. In order to further understand the effect of carbon black, we tested the square rsesistance of 5 μm thick CCEs with different content of carbon black, which are represented in **Table 2**. It is clear that the square resistance of CCEs increase gradually with the content of carbon black was increased. The decreased J_{sc} and *FF* for devices with high contents of carbon black in CCEs is probably due to the high square resistance of CCEs, which subsequently results in decreased charge colltion efficiency.

The long-term stability in the dark of devices based on graphite/carbon black CE with the initial efficiency of 5.52% was tested under conditions stored in air atmosphere at room temperature without encapsulation and presented in **Fig. 7**. It could be found that

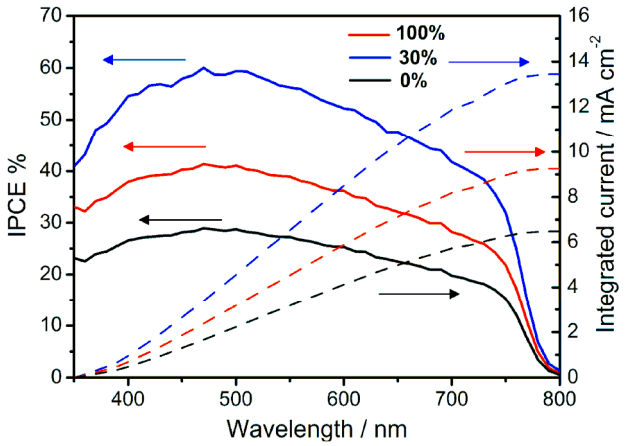

Fig. 6 IPCE curves for devices based on CEs with 0%(black curve), 30%(blue curve) and 100%(red curve) contents of carbon black respectively. The integrated photocurrents calculated from the overlap integral of the IPCE spectra with the AM 1.5 solar emission.

Table 2 Square sesistance of 5 μm thick CCEs with different contents of carbon black in CCEs.

	0%	10%	20%	30%	100%
R_{sq}(Ω)	40.4	76.4	114.4	164.4	864.4

after more than 900 hours, although the J_{sc} decreased slightly, the PCE still remained over 5.5%.These results indicate the superior stability of $CH_3NH_3PbI_3/TiO_2$ heterojunction solar cells based on CCEs.

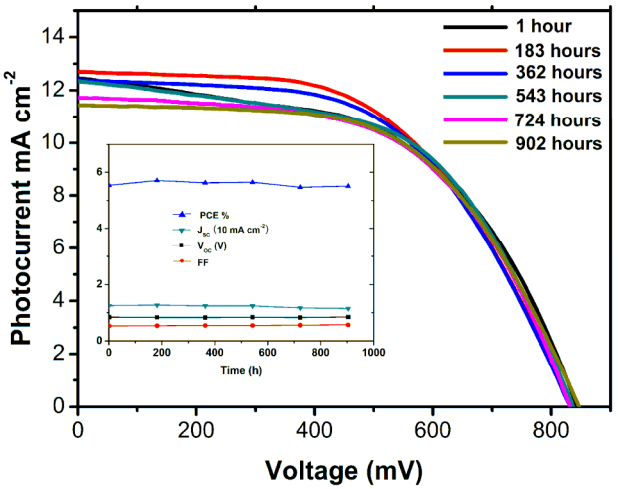

Fig. 7 Long term stability at room temperature in the dark. Inset: the changing characters of the device in 902 h after been fabricated.

Conclusions

In conclusion, as one of the main components in CCEs, carbon black has significant influence not only on the conductivity of CCEs but also on the crystallinity and uniformity of $CH_3NH_3PbI_3$ deposited on CCEs, which will eventually affect the photovoltaic performance of devices. Devices based on graphite/carbon black CEs with different

contents of carbon black were made to study the influence of carbon black. Results show that carbon black could decrease the crystallinity of $CH_3NH_3PbI_3$ crystallites and improve uniformity of $CH_3NH_3PbI_3$ film on CCEs, leading to improved photovoltaic performance for mesoscopic $CH_3NH_3PbI_3/TiO_2$ heterojunction solar cells.

Acknowledgements

The authors acknowledge the financial support from National Natural Science Foundation of China (No.11404279). We thank the experiment center of Yancheng Teachers University for field emission scanning electron microscopy (FE-SEM) testing. We thank Michael Grätzel Center for Mesoscopic Solar Cells of Wuhan National Laboratory for Optoelectronics for Current–voltage characterization and IPCE curves testing.

Notes and references

Department of new energy, School of Physical Science and Electronic Technology, Yancheng Teachers University, Yancheng, Jiangsu, P.R. China, 224000. E-mail: wangheng8463@163.com; Tel: +86 0515 8825 8236

1. A. Kojima, K. Teshima, Y. Shirai and T. Miyasaka, *J. Am. Chem. Soc.*, 2009, **131**, 6050.
2. J. H. Im, C. R. Lee, J. W. Lee, S. W. Park and N. G. Park, *Nanoscale*, 2011, **3**, 4088.
3. H.-S. Kim, C.-R. Lee, J.-H. Im, K.-B. Lee, T. Moehl, A. Marchioro, S.-J. Moon, R. Humphry-Baker, J.-H. Yum, J. E. Moser, M. Grätzel and N.-G. Park, *Sci. Rep.*, 2012, **2**.
4. M. M. Lee, J. Teuscher, T. Miyasaka, T. N. Murakami and H. J. Snaith, *Science*, 2012, **338**, 643.
5. H. Chen, X. Pan, W. Liu, M. Cai, D. Kou, Z. Huo, X. Fang and S. Dai, *Chem. Commun.*, 2013, **49**, 7277.
6. B. Cai, Y. Xing, Z. Yang, W.-H. Zhang and J. Qiu, *Energy Environ. Sci.*, 2013, **6**, 1480.
7. W. A. Laban and L. Etgar, *Energy Environ. Sci.*, 2013, **6**, 3249.
8. Z. Xiao, C. Bi, Y. Shao, Q. Dong, Q. Wang, Y. Yuan, C. Wang, Y. Gao and J. Huang, *Energy Environ. Sci.*, 2014, **7**, 2619.
9. N. J. Jeon, J. H. Noh, Y. C. Kim, W. S. Yang, S. Ryu and S. I. Seok, *Nat. Mater.*, 2014.
10. H. Zhou, Q. Chen, G. Li, S. Luo, T.-b. Song, H.-S. Duan, Z. Hong, J. You, Y. Liu and Y. Yang, *Science*, 2014, **345**, 542.
11. M. Liu, M. B. Johnston and H. J. Snaith, *Nature*, 2013, **501**, 395.
12. J. Burschka, N. Pellet, S.-J. Moon, R. Humphry-Baker, P. Gao, M. K. Nazeeruddin and M. Grätzel, *Nature*, 2013, **499**, 316.
13. Z. Ku, Y. Rong, M. Xu, T. Liu and H. Han, *Sci. Rep.*, 2013, **3**.
14. A. Mei, X. Li, L. Liu, Z. Ku, T. Liu, Y. Rong, M. Xu, M. Hu, J. Chen, Y. Yang, M. Grätzel and H. Han, *Science*, 2014, **345**, 295.
15. L. Zhang, T. Liu, L. Liu, M. Hu, Y. Yang, A. Mei and H. Han, *J. Mater. Chem. A*, 2015.
16. Z. Huang, X. Liu, K. Li, D. Li, Y. Luo, H. Li, W. Song, L. Chen and Q. Meng, *Electrochem.Commun.*, 2007, **9**, 596.
17. A. Kay and M. Grätzel, *Sol. Energ. Mat. and Sol. C.*, 1996, **44**, 99.
18. Y. Wu, A. Islama, X. Yang, C. Qin, J. Liu, K. Zhang, W. Peng and L. Han, *Energy Environ. Sci.*, 2014, **7**, 2934.
19. G. Liu, H. Wang, X. Li, Y. Rong, Z. Ku, M. Xu, L. Liu, M. Hu, Y. Yang, P. Xiang, T. Shu, H. Han, *Electrochim. Acta*, 2012, **69**, 334.